Heterogeneous Catalysis

Deutsche Ausgabe: DOI: 10.1002/ange.201605215
Internationale Ausgabe: DOI: 10.1002/anie.201605215

Visualizing Dealumination of a Single Zeolite Domain in a Real-Life Catalytic Cracking Particle

*Sam Kalirai, Pasi P. Paalanen, Jian Wang, Florian Meirer, and Bert M. Weckhuysen**

Abstract: *Fluid catalytic cracking (FCC) catalysts play a central role in the chemical conversion of crude oil fractions. Using scanning transmission X-ray microscopy (STXM) we investigate the chemistry of one fresh and two industrially deactivated (ECAT) FCC catalysts at the single zeolite domain level. Spectro-microscopic data at the Fe L_3, La M_5, and Al K X-ray absorption edges reveal differing levels of deposited Fe on the ECAT catalysts corresponding with an overall loss in tetrahedral Al within the zeolite domains. Using La as a localization marker, we have developed a novel methodology to map the changing Al distribution of single zeolite domains within real-life FCC catalysts. It was found that significant changes in the zeolite domain size distributions as well as the loss of Al from the zeolite framework occur. Furthermore, inter- and intraparticle heterogeneities in the dealumination process were observed, revealing the complex interplay between metal-mediated pore accessibility loss and zeolite dealumination.*

Fluid catalytic cracking (FCC), one of the world's major industrial chemical conversion processes, is used to crack heavy hydrocarbon feedstocks into more valuable products, such as gasoline and propylene.[1] The process utilizes hierarchically structured, 50–150 μm-sized catalyst particles composed of silica, alumina, clay, and zeolite materials. The main activity of the catalyst arises from the zeolite phase, which in turn is the result of Al atoms present in the tetrahedral sites of the zeolite framework where the resulting negative charge is compensated by Brønsted acidic hydrogen atoms. During FCC, the harsh hydrothermal conditions of the regenerator, in which coke is burned and acidity is restored, result in a degradation of the zeolite through migration of framework Al (FAL) to extra-framework (EFAL) and non-framework sites corresponding to an irreversible loss in catalytic activity.[2] In order to mitigate these aging effects, FCC catalysts typically use modified, rare-earth (i.e. La) incorporated zeolite Y that provide higher hydrothermal stability.[3,4] Due to their vital industrial role, understanding and reducing zeolite dealumination and the factors influencing the degradation of zeolite Y in the presence of metal poisons and steam remains one of the most important topics related to catalyst design.[5–7]

To this end, spectroscopic techniques, such as solid-state NMR and X-ray absorption near edge structure (XANES) spectroscopies, play a central role in characterizing the nature and formation of EFAL in steamed zeolites.[8–13] For example, van Bokhoven et al. have shown that it is possible to track the changes in Al coordination upon in situ steaming of zeolite beta using Al K-edge XANES.[12] However, these spectroscopic techniques are inevitably limited to single zeolite component systems, thus neglecting the chemical complexity of hierarchical multi-component catalyst materials, of which real-life FCC catalyst particles are a clear showcase system.[14,15]

In order to understand zeolite activity in the context of FCC catalysis, where matrix and binder materials play a key role, characterization techniques that possess both spatial and chemical information are required. In this regard, chemical insight may be achieved using X-ray microscopy techniques, which combines the chemical sensitivity of XANES with high (that is, down to ca. 10–30 nm) spatial resolution.[16–23] One such technique, namely soft X-ray scanning transmission X-ray microscopy (STXM), has been successfully used to elucidate both spatial and chemical behavior of isolated steamed and dealuminated zeolites, but has never been extended to study multi-component and hierarchically structured zeolite-based catalysts.[24–28]

Here, we present a first-of-its-kind study in which we used STXM to probe zeolite dealumination within real-life fresh and genuine, industrially deactivated FCC catalysts at the size regime of a single zeolite domain. The experimental approach of the study is illustrated in Figure 1. To measure the FCC catalyst particles in STXM transmission mode, one fresh and two industrially deactivated equilibrium catalyst (ECAT) samples were microtomed to 500 nm-thin sections (Figure 1a). The two ECAT particles are further denoted as ECAT1 and ECAT2. With STXM, spectromicroscopic maps over whole catalyst particle thin sections with 100×100 nm pixel size were captured with a field-of-view encompassing each particle thin section (40 to 50 μm; Figure 1b).[19] Elemental maps of Fe (L_3 edge), La (M_5 edge) and Al (K edge) were captured to map the distribution of deposited metals (i.e. Fe) and to visualize the zeolite and matrix domains (by La and Al; Figure 1c). In contrast to the fresh

[*] S. Kalirai, P. P. Paalanen, Dr. F. Meirer, Prof. Dr. B. M. Weckhuysen
Inorganic Chemistry and Catalysis group
Debye Institute for Nanomaterials Science
Utrecht University
Universiteitsweg 99, 3584 CG Utrecht (The Netherlands)
E-mail: b.m.weckhuysen@uu.nl
Dr. J. Wang
Canadian Light Source Inc., University of Saskatchewan
44 Innovation Blvd., Saskatoon, SK, S7N 2V3 (Canada)

Supporting information for this article can be found under: http://dx.doi.org/10.1002/anie.201605215.

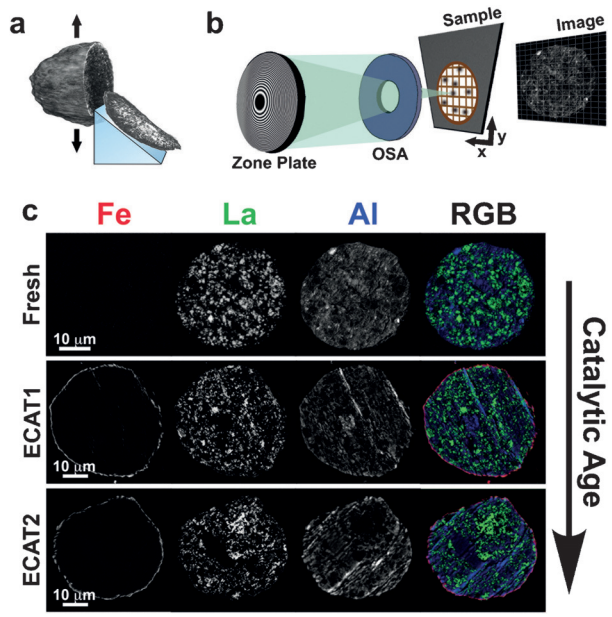

Figure 1. a) Fluid catalytic cracking (FCC) particles were microtomed to 500 nm thin sections. b) Scanning transmission X-ray microscopy (STXM) uses focused X-rays from a zone plate to form a point-by-point image such that the field-of-view is adjustable. Varying the incoming X-ray energy across an absorption edge yields X-ray spectroscopic information at each pixel. c) STXM maps of Al, La, Fe, and the corresponding RGB overlay show how STXM is used to correlate the zeolite Al chemistry with the catalytic age as determined by metal deposition.

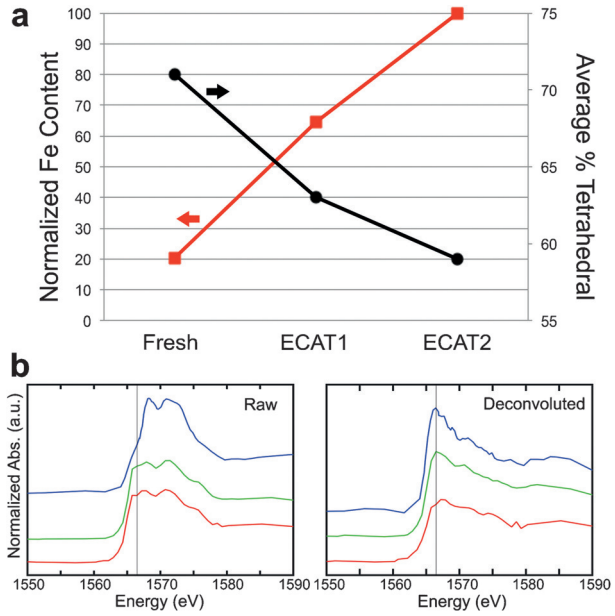

Figure 2. a) The average Fe content (black dots) of each catalyst particle was determined so as to classify the relative catalytic age of the three catalyst particles under study. Concurrently, the zeolite domains show a loss in the average % tetrahedral Al present as a function of catalytic age. The average % tetrahedral Al was determined by inspecting the Al K-edge XANES of the zeolite domains. b) The average raw (left) and deconvoluted (right) Al K-edge XANES from zeolite domains in the fresh (blue), ECAT1 (green) and ECAT2 (red) particles. After deconvolution, the XANES of the fresh particle closely resembles that of a measured zeolite Y reference spectrum (see Figure S7).

catalyst particle, the ECAT particles contain an Fe shell on the catalyst perimeter that is deposited from the crude oil feedstock confirming that they have undergone aging.[29,30] The relative age of the two ECAT particles are unknown, however by using the concentration of Fe present in each particle the relative catalytic age can be determined.[31] Using this approach (see the Supporting Information), it was found that the ECAT2 particle is "catalytically older" than the ECAT1 particle due to its higher mean Fe loading (Figure 2a, black dots). This observation was further confirmed with 2D XRF measurements where the amount of deposited metal poisons, that is, Fe, Ni, and Ca, are higher in ECAT2 than in ECAT1 (see Figures S1 and S2 in the Supporting Information).

We were then able to determine the degree of dealumination within zeolite domains in the three, now age-classified FCC catalyst particles by developing a procedure to visualize the individual zeolite Y domains within the FCC matrix by using La as a quantitative marker. Transmission experiments yield projection images of the 500 nm thick sample, where the spot signal associated with the zeolite domains within the FCC particle is convoluted with the signal from the embedding matrix. By using the fact that the La content in the zeolites provides an accurate means of determining the fractional amount of zeolite in a single spot, we were able to isolate the XANES signal corresponding to the zeolite (Figure 2). Details of this method can be found in the Supporting Information (Figures S3–5). After deconvolution, the average spectra of the masked zeolite regions within the fresh FCC catalyst particle closely resemble that of a measured reference zeolite Y spectrum (Figure 2b, Figures S6–9). The peak shift towards higher energy and the appearance of secondary peaks is consistent with previously observed transformations of tetrahedrally coordinated Al (i.e. framework Al) species to octahedrally coordinated Al (i.e. extra-framework Al) species in steamed zeolites.[8,32] Subsequently, a non-negative linear combination least-squares fit was performed with three reference compounds: that is, pure 4-coordinated Al (ZSM-5), α-alumina (6-coordinated Al, oxide), and boehmite (6-coordinated Al, oxyhydroxide). ZSM-5 was chosen for the fit as it has a near identical spectral profile with zeolite Y while only containing tetrahedrally coordinated Al (whereas commercial zeolite Y often contains a mixture of tetrahedral and octahedral Al).[33] It was found that the aging trends, as determined by the increasing metals content in each FCC catalyst particle, correspond very well with a decrease in the amount of tetrahedrally coordinated Al (Figure 2b). The fit yields coefficients of determinations 0.97, 0.96, and 0.92 for the Fresh, ECAT1 and ECAT2 particles, respectively, showing that the model explains the majority of the variance in the spectra. This observation underlines the overall framework dealumination of the zeolite domains within the ECAT1 and ECAT2 particles and represents the first direct observation of the complex zeolite dealumination processes taking place within real-life FCC catalyst particles at the level of a single

zeolite domain. In addition to the observed transformations in the zeolite chemistry, a fitting of the catalyst matrix also showed chemical changes (Figure S11) similar to those previously reported in the literature.[34]

In a third step, binary maps created from the La elemental maps (Figure 3a) were used to determine the size and

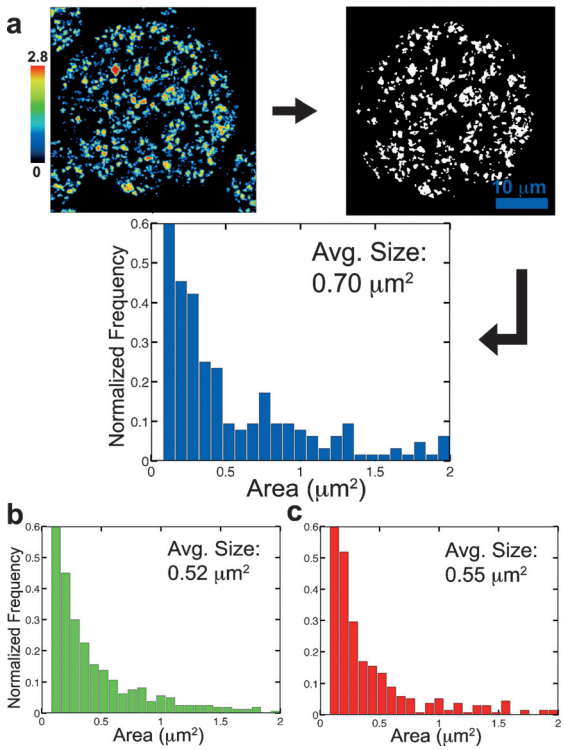

Figure 3. The La M_5-edge map was used to create a binary mask of the individual zeolite domains within each FCC particle using a ΔOD threshold selection of 1.2. The resulting histograms of zeolite domain sizes plotted for the a) fresh, b) ECAT1, and c) ECAT2 catalyst particles.

location of individual zeolite domains for the FCC catalyst particles under study. It was found that the average size of a zeolite aggregate domain for the fresh FCC catalyst particle (0.70 µm², Figure 3a) is significantly larger than that of the ECAT1 (0.52 µm², Figure 3b) and ECAT2 (0.55 µm², Figure 3c) particles. The observed zeolite size distributions are consistent with other studies where conventional and single-molecule confocal fluorescence microscopy were used to study FCC catalysts containing ZSM-5 zeolites, thus supporting the use of La as a specific marker for pinpointing individual zeolite domains in a catalyst matrix.[35,36]

Lastly, we extended the developed approach to determine the relative percentage of tetrahedrally coordinated Al of individual zeolite domains within each particle (Figure 4). By performing segmentation on a zeolite-by-zeolite basis, we were able to extract the Al K-edge XANES of each domain within the catalyst particle. To ensure sufficient signal-to-noise ratio of the XANES, only zeolite domains that were larger than 25 pixels were considered. The resulting XANES of domains within this criterion were then fitted, as above, to estimate the fractional amount of tetrahedral and octahedral Al present. The histograms plotting the percentage frequency of zeolite aggregate domains for a given tetrahedral Al percent range and spatial maps are shown in Figure 4. As expected, the histogram of the fresh catalyst particle exhibits a narrow distribution for the percentage of tetrahedral Al, where the majority of domains fall within the range of 60–80% for tetrahedral Al and the highest percentage frequency is at 70–75% with a mean value of 71%. In contrast, it was found that the mean value ECAT1 is 64% for tetrahedral Al and for ECAT2 it is 58%, while the dispersions in both ECAT catalyst particles are significantly higher than in the fresh one. The zeolite aggregate domains in the 70–75% range, which was the highest for the fresh catalyst particle, represents less than 10% of the total in ECAT2. The spatial map corresponding to the percentage of tetrahedral Al in each domain reflects the differences observed in the histogram. Moreover, in the ECAT particles, lower fractional tetrahedral Al domains appear to be present in discrete zones on the lower portion of the particle. Coupled with the observation that the fresh particle is largely homogeneous, this suggests that these heterogeneities arise only during aging in the FCC reactor. We posit that these differences may be linked to differences in interparticle accessibility resulting from metal deposition, thus playing a synergistic role in catalytic aging by dealumination and accessibility loss.

In summary, STXM quantitatively visualizes the size and Al chemistry of individual zeolite domains dispersed within real-life FCC catalyst particles upon aging. This approach relies on the exclusivity of La to the domains of zeolite Y, thereby serving as a quantitative marker to deconvolute the zeolite aggregates from the complex matrix and binder chemistry of an FCC catalyst particle. It was found that upon increased metal deposition by catalyst poisoning significant chemical transformations occur within the zeolite domains corresponding to framework dealumination. Furthermore, the observed spatial heterogeneities during this aging process indicate that zeolite dealumination does not occur homogeneously throughout single catalyst particles. Finally, this study demonstrates that the STXM method moves the in-depth investigation of zeolite-based catalyst deactivation processes from single-component catalyst systems into the realm of complex, multi-component and hierarchically structured catalyst materials of direct industrial relevance.

Acknowledgements

This work is supported by the NWO Gravitation program, Netherlands Center for Multiscale Catalytic Energy Conversion (MCEC) and a European Research Council (ERC) Advanced Grant (grant number 321140). We thank Albemarle for providing the FCC samples. This research was performed at CLS, which is supported by the Canada Foundation for Innovation, Natural Sciences and Engineering Research Council of Canada, the University of Saskatchewan, the Government of Saskatchewan, Western Economic Diversification Canada, the National Research Council Canada,

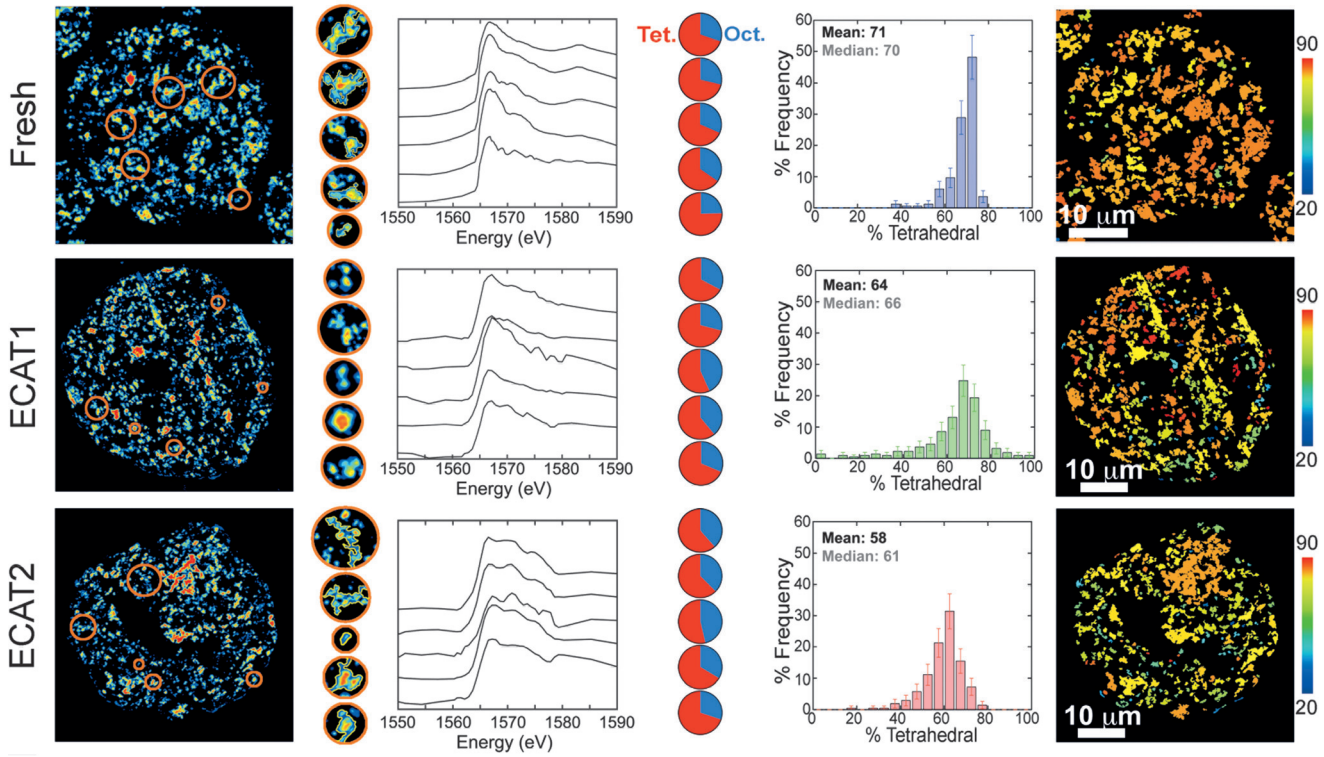

Figure 4. The tetrahedral versus octahedral Al present in individual zeolite domains is illustrated from left to right for Fresh (top), ECAT1 (middle) and ECAT2 (bottom) particles. Segmentation of the La map yields individually segmented domains from which the average deconvoluted XANES spectrum was determined. In the second panel (from the left) of the figure, five selected zeolite domains and their corresponding Al K-edge XANES are shown. These spectra were then individually fit using the three reference Al compounds (namely, ZSM-5, α-alumina and boehmite) to determine the amount of tetrahedral and octahedral Al present in each zeolite, as shown by the corresponding pie charts (red: tetrahedral %, blue: octahedral %). For each segmented domain within the particle, the % tetrahedral Al per zeolite is plotted as a histogram to show the distribution between zeolites within the particle. Finally this distribution is also plotted spatially (from the range 20% to 90%) such that the color of each domain corresponds to the respective amount of tetrahedral Al as determined by the fit.

and the Canadian Institutes of Health Research. We thank J.D. Meeldijk (Utrecht University) for preparing the sectioned catalysts and W. de Nolf (ESRF) for collecting and processing the 2D XRF data.

Keywords: dealumination · fluid catalytic cracking · heterogeneous catalysis · X-ray microscopy · zeolites

How to cite: *Angew. Chem. Int. Ed.* **2016**, *55*, 11134–11138
Angew. Chem. **2016**, *128*, 11300–11304

[1] E. T. C. Vogt, B. M. Weckhuysen, *Chem. Soc. Rev.* **2015**, *44*, 7342–7370.
[2] H. S. Cerqueira, G. Caeiro, L. Costa, F. Ramôa Ribeiro, *J. Mol. Catal. A* **2008**, *292*, 1–13.
[3] J. Scherzer, R. E. Ritter, *Ind. Eng. Chem. Prod. Res. Dev.* **1978**, *17*, 219–223.
[4] F. E. Trigueiro, D. F. J. Monteiro, F. M. Z. Zotin, E. Falabella Sousa-Aguiar, *J. Alloys Compd.* **2002**, *344*, 337–341.
[5] S. Li, A. Zheng, Y. Su, H. Zhang, L. Chen, J. Yang, C. Ye, F. Deng, *J. Am. Chem. Soc.* **2007**, *129*, 11161–11171.
[6] Z. Yu, A. Zheng, Q. Wang, L. Chen, J. Xu, J.-P. Amoureux, F. Deng, *Angew. Chem. Int. Ed.* **2010**, *49*, 8657–8661; *Angew. Chem.* **2010**, *122*, 8839–8843.
[7] J. A. van Bokhoven, H. Sambe, D. E. Ramaker, D. C. Koningsberger, *J. Phys. Chem. B* **1999**, *103*, 7557–7564.
[8] G. Agostini, C. Lamberti, L. Palin, M. Milanesio, N. Danilina, B. Xu, M. Janousch, J. A. van Bokhoven, *J. Am. Chem. Soc.* **2010**, *132*, 667–678.
[9] R. D. Shannon, K. H. Gardner, R. H. Staley, G. Bergeret, P. Gallezot, A. Auroux, *J. Phys. Chem.* **1985**, *89*, 4778–4788.
[10] A. Omegna, R. Prins, J. A. van Bokhoven, *J. Phys. Chem. B* **2005**, *109*, 9280–9283.
[11] J. A. van Bokhoven, A. M. J. Van der Eerden, D. C. Koningsberger, *J. Am. Chem. Soc.* **2003**, *125*, 7435–7442.
[12] J. A. van Bokhoven, D. C. Koningsberger, P. Kunkeler, H. van Bekkum, *J. Catal.* **2002**, *211*, 540–547.
[13] J. A. van Bokhoven, C. Lamberti, *Coord. Chem. Rev.* **2014**, *277–278*, 275–290.
[14] S. Mitchell, N.-L. Michels, J. Pérez-Ramírez, *Chem. Soc. Rev.* **2013**, *42*, 6094–6112.
[15] N. Hosseinpour, Y. Mortazavi, A. Bazyari, A. A. Khodadadi, *Fuel Process. Technol.* **2009**, *90*, 171–179.
[16] A. M. Beale, S. D. M. Jacques, E. K. Gibson, M. Di Michiel, *Coord. Chem. Rev.* **2014**, *277–278*, 208–223.
[17] S. W. T. Price, K. Geraki, K. Ignatyev, P. T. Witte, A. M. Beale, J. F. W. Mosselmans, *Angew. Chem. Int. Ed.* **2015**, *54*, 9886–9889; *Angew. Chem.* **2015**, *127*, 10024–10027.
[18] A. M. Beale, S. D. M. Jacques, B. M. Weckhuysen, *Chem. Soc. Rev.* **2010**, *39*, 4656–4672.
[19] K. V. Kaznatcheev, C. Karunakaran, U. D. Lanke, S. G. Urquhart, M. Obst, A. P. Hitchcock, *Nucl. Instrum. Methods Phys. Res. Sect. B* **2007**, *582*, 96–99.

[20] J.-D. Grunwaldt, B. Kimmerle, A. Baiker, P. Boye, C. G. Schroer, P. Glatzel, C. N. Borca, F. Beckmann, *Catal. Today* **2009**, *145*, 267 – 278.
[21] S. Bordiga, F. Bonino, K. P. Lillerud, C. Lamberti, *Chem. Soc. Rev.* **2010**, *39*, 4885 – 4927.
[22] J.-D. Grunwaldt, C. G. Schroer, *Chem. Soc. Rev.* **2010**, *39*, 4741 – 4753.
[23] S. R. Bare, M. E. Charochak, S. D. Kelly, B. Lai, J. Wang, Y. K. Chen-Wiegart, *ChemCatChem* **2014**, *6*, 1427 – 1437.
[24] H. E. van der Bij, F. Meirer, S. Kalirai, J. Wang, B. M. Weckhuysen, *Chem. Eur. J.* **2014**, *20*, 16922 – 16932.
[25] H. E. Van Der Bij, L. R. Aramburo, B. Arstad, J. J. Dynes, J. Wang, B. M. Weckhuysen, *ChemPhysChem* **2014**, *15*, 283 – 292.
[26] H. E. van der Bij, D. Cicmil, J. Wang, F. Meirer, F. M. F. de Groot, B. M. Weckhuysen, *J. Am. Chem. Soc.* **2014**, *136*, 17774 – 17787.
[27] L. R. Aramburo, Y. Liu, T. Tyliszczak, F. M. F. De Groot, J. C. Andrews, B. M. Weckhuysen, *ChemPhysChem* **2013**, *14*, 496 – 499.
[28] L. R. Aramburo, E. De Smit, B. Arstad, M. M. Van Schooneveld, L. Sommer, A. Juhin, T. Yokosawa, H. W. Zandbergen, U. Olsbye, F. M. F. De Groot, B. M. Weckhuysen, *Angew. Chem. Int. Ed.* **2012**, *51*, 3616 – 3619; *Angew. Chem.* **2012**, *124*, 3676 – 3679.
[29] a) F. Meirer, S. Kalirai, D. Morris, S. Soparawalla, Y, Liu, G. Mesu, J. C. Andrews, B. M. Weckhuysen, *Sci. Adv.* **2015**, *1*, e1400199; b) F. Meirer, D. T. Morris, S. Kalirai, Y. Liu, J. C. Andrews, B. M. Weckhuysen, *J. Am. Chem. Soc.* **2015**, *137*, 102 – 105; c) F. Meirer, S. Kalirai, J. N. Weker, Y. Liu, J. C. Andrews, B. M. Weckhuysen, *Chem. Commun.* **2015**, *51*, 8097 – 8100.
[30] a) S. Kalirai, U. Boesenberg, G. Falkenberg, F. Meirer, B. M. Weckhuysen, *ChemCatChem* **2015**, *7*, 3674 – 3682; b) A. M. Wise, J. N. Weker, S. Kalirai, M. Farmand, D. A. Shapiro, F. Meirer, B. M. Weckhuysen, *ACS Catal.* **2016**, *6*, 2178 – 2181.
[31] O. Bayraktar, E. L. Kugler, *Catal. Lett.* **2003**, *90*, 155 – 160.
[32] P. Ildefonse, D. Cabaret, P. Sainctavit, G. Calas, A. M. Flank, P. Lagarde, *Phys. Chem. Miner.* **1998**, *25*, 112 – 121.
[33] I. J. Drake, Y. Zhang, M. K. Gilles, C. N. Teris Liu, P. Nachimuthu, R. C. C. Perera, H. Wakita, A. T. Bell, *J. Phys. Chem. B* **2006**, *110*, 11665 – 11676.
[34] J. Ruiz-Martínez, A. M. Beale, U. Deka, M. G. O'Brien, P. D. Quinn, J. F. W. Mosselmans, B. M. Weckhuysen, *Angew. Chem. Int. Ed.* **2013**, *52*, 5983 – 5987; *Angew. Chem.* **2013**, *125*, 6099 – 6103.
[35] C. Sprung, B. M. Weckhuysen, *Chem. Eur. J.* **2014**, *20*, 3667 – 3677.
[36] Z. Ristanović, M. M. Kerssens, A. V. Kubarev, F. C. Hendriks, P. Dedecker, J. Hofkens, M. B. J. Roeffaers, B. M. Weckhuysen, *Angew. Chem. Int. Ed.* **2015**, *54*, 1836 – 1840; *Angew. Chem.* **2015**, *127*, 1856 – 1860.

Received: May 28, 2016
Published online: July 6, 2016

